Acta Pharmacologica Sinica (2017) 38: 954–962
 1671-4083/17
www.nature.com/aps

Original Article

Claudin 4-targeted nanographene phototherapy using a *Clostridium perfringens* enterotoxin peptide-photosensitizer conjugate

Gayong SHIM[#], Mi-Gyeong KIM[#], Hyerim JIN, Jinyoung KIM, Yu-Kyoung OH*

College of Pharmacy and Research Institute of Pharmaceutical Sciences, Seoul National University, Seoul 08826, Republic of Korea

Abstract

In this study we designed a claudin 4-directed dual photodynamic and photothermal system, in which a 30-amino acid claudin 4-binding peptide, *Clostridium perfringens* enterotoxin (CPE), was linked to a photodynamic agent chlorin e6 (Ce6) through a polyethylene glycol spacer (CPC) and anchored onto reduced graphene oxide (rGO) nanosheets to form CPC/rGO nanosheets. For comparison, a conjugate of polyethylene glycol and Ce6 (PC) was anchored onto the rGO nanosheets to generate PC/rGO. Both PC and CPC generated reactive oxygen species upon irradiation at 660 nm. Application of CPC/rGO to claudin 4-overexpressing U87 glioblastoma cells *in vitro* resulted in a significantly higher cellular uptake compared to application of PC/rGO. Upon irradiation at 660 and 808 nm, the CPC/rGO-treated U87 cells generated significantly higher reactive oxygen species and caused significantly higher temperature increase, and showed most potent anticancer effect compared to the other groups. Taken together, these results suggest that CPC/rGO is potentially useful as a tumor-specific combined phototherapy.

Keywords: photodynamic therapy; photothermal therapy; *Clostridium perfringens* enterotoxin; claudin 4; reduced graphene oxide; U87 glioblastoma cells

Acta Pharmacologica Sinica (2017) 38: 954–962; doi: 10.1038/aps.2017.46; published online 22 May 2017

Introduction

Photoresponsive therapy has attracted tremendous interest as a minimally invasive method to treat malignant tissues with the potential for fewer complications than typical conventional surgery and chemotherapy[1, 2]. Photodynamic therapy (PDT) employs photosensitizers (PSs) and specific visible light irradiation to generate reactive oxygen species (ROS) that are locally cytotoxic to target sites[2]. Photothermal therapy (PTT) utilizes photoresponsive agents that can absorb near-infrared (NIR) light and generate heat, leading to hyperthermia-induced cell death at target sites[1]. Although the above treatment modalities have been enthusiastically studied for use in cancer treatment, they are limited by their distribution to normal tissue due to the non-selective cellular uptake of photoresponsive agents[3]. To minimize side effects and reduce the effective dosage, photodynamic therapies must be able to target tumor cells[4].

Overexpression of claudin 4 receptors has been observed in many types of tumor cells and is known to contribute to the development of cancers[5]. *Clostridium perfringens* enterotoxin (CPE), a potent cytolytic toxin, is a ligand of the claudin 4 receptors[6]. A carboxy-terminal fragment of CPE has been used to bind claudin 4 receptors on the surfaces of target cells because full-length CPE has lethal effects[7]. The use of CPE as a targeting moiety for a nanocarrier has not yet been extensively investigated.

A variety of photoresponsive agents, such as carbon[8, 9], gold[10], and polypyrrole[11]-based nanomaterials, have been studied for use in photothermal therapy. Among these, graphene-based nanosheets are advantageous for photothermal cancer treatment by virtue of their large infrared absorption coefficient compared to other light absorbers[8]. The planar hydrophobic structure of graphene permits covalent or non-covalent functionalization to load a multi-functional agent[12]. Although nano-graphenes have intrinsic photothermal activity, PSs non-covalently loaded onto graphene nanosheets might reduce the graphene dose and allow implementation of a dual-phototherapy approach through excitation at two wavelengths.

Graphene nanosheet-based dual phototherapy has been studied using PSs such as chlorin e6 (Ce6) and methylene

[#]These authors contributed equally to this article.
*To whom correspondence should be addressed.
E-mail ohyk@snu.ac.kr
Received 2017-01-09 Accepted 2017-04-24

blue[13, 14]. Ce6, one widely used PS in phododynamic therapy[15], was loaded to polyethylene glycol (PEG)-functionalized graphene nanosheets for dual phototherapy[13]. Methylene blue complexed to nonionic triblock copolymer-functionalized graphene nanosheets was shown to provide synergistic antitumor effects after irradiation at two wavelengths for photodynamic and photothermal therapy[14]. Although these studies demonstrate the potential of dual phototherapy, surface modification of graphene-based nanosheets with tumor-targeting molecules may further improve the antitumor efficacy of dual phototherapy.

Here, we report that tethering a claudin 4-binding peptide onto reduced graphene (rGO) nanosheets using a PS as an anchoring moiety improved targeted delivery to claudin 4-overexpressing cells. rGO exerted both photodynamic and photothermal anticancer effects upon irradiation at two wavelengths. The operational mechanisms and a schematic diagram of the PC/rGO and CPC/rGO systems are illustrated in Figure 1. In this system, Ce6 was used to photosensitize PDT and act as a tethering moiety to bind the claudin 4-targeting peptide onto the graphene nanosheets.

Materials and methods

Synthesis of CPE30 conjugates with PEG and Ce6

A mixture of Ce6 (20 mg, 0.034 mmol; Frontier Scientific, Inc, Salt Lake City, UT, USA), amine-PEG2000-Boc (0.9 eq; Nanocs Inc, New York, NY, USA), N-ethyl-N'-(3-dimethylaminopropyl) carbodiimide (2 eq; Sigma–Aldrich, St Louis, MO, USA), hydroxybenzotriazole (2 eq; Sigma–Aldrich) and N,N-diisopropylethylamine (4 eq; Sigma–Aldrich) were dissolved in dimethyl formamide (3 mL; Sigma–Aldrich) and stirred at room temperature. After 24 h, the reaction product, a conjugate of Ce6 with PEG (PC conjugate), was purified using a dialysis membrane (Spectra/Por, molecular weight cutoff size, 1000; Rancho Dominguez, CA, USA) against phosphate-buffered saline with 0.2% Tween 80 (pH 7.4, PBS-T) and deionized water over 2 d and lyophilized until use[16].

The PEG moiety conjugated to Ce6 and CPE30 at either end (the CPC conjugate) was synthesized by first linking PEG to the C-terminus of the 30 residue sequence of CPE (CPE30, SLDAGQYVLVMKANSSYSGNYPYSILFQKF). In brief, a mixture of CPE30 (20 mg; Peptron, Daejeon, Republic of Korea), succinimidyl-PEG-Boc (1.1 eq; Sigma–Aldrich), and N,N-diisopropylethylamine (4 eq; Sigma–Aldrich) was dissolved in dimethyl formamide (3 mL; Sigma–Aldrich) and stirred at room temperature. After 24 h, the conjugate of CPE30 to PEG was purified using a dialysis membrane (Spectra/Por, molecular weight cutoff size, 3500) against deionized water over 2 d, followed by lyophilization. The resulting conjugate of CPE30 and PEG was then dissolved in trifluoroacetic acid/dichloro-

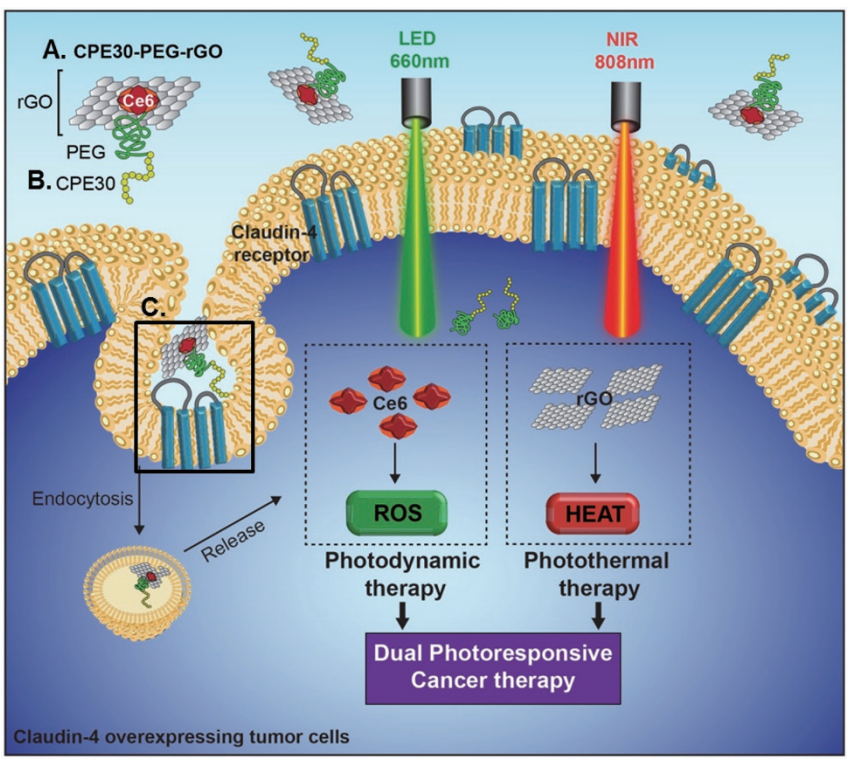

Figure 1. Dual-photoresponsive cancer therapy: CPC/rGO on claudin 4-overexpressing cancer cells. Schematic diagram showing the CPC/rGO (A) nanosheets. CPC/rGO was composed of the targeting ligand, the photothermal rGO, and the PS Ce6 as an anchoring moiety. CPC/rGO may enter the cells via claudin 4-mediated endocytosis due to the presence of the CPE30 ligand (B). Box (C) illustrates that CPE30 specifically binds to the secondary loop of the claudin 4 receptor, which extends into the extracellular matrix. Irradiation at 660 nm induces ROS generation by Ce6 to apply photodynamic anticancer activity. Irradiation at 808 nm enabled the rGO nanosheets to exert photothermal anticancer activity.

methane (1:1, 10 mL) and stirred at room temperature. After 3 h, the mixture was evaporated in vacuo and mixed with Ce6 (1.1 eq), N-ethyl-N2-(3-dimethylaminopropyl) carbodiimide (1 eq), hydroxybenzotriazole (1 eq) and N,N-diisopropylethylamine (4 eq) in dimethylformamide. The coupling reaction proceeded over 72 h at room temperature, after which, the resulting CPC conjugate was dialyzed against an excess of PBS-T and deionized water using a dialysis membrane (Spectra/Por, molecular weight cutoff size, 1000) and then lyophilized.

Preparation of CPE30-tethered rGO

rGO nanosheets were prepared using a modified Hummer's method, as described previously[17]. The rGO surfaces were coated with PC conjugate or CPC conjugate by mixing rGO nanosheets in deionized water (1 mg/mL) with the same volume of PC conjugate (4.2 mmol/L) or CPC conjugate (4.2 mmol/L). PC-loaded rGO (PC/rGO) or CPC-loaded rGO (CPC/rGO) were then purified by an Amicon Ultra centrifugal filter (MWCO 100K; Millipore, Darmstadt, Germany) via centrifugation at 1600×*g* for 30 min. Due to the quenching of the conjugates on rGO nanosheets, the loading amounts of PC or CPC on rGO nanosheets were measured by assaying the amounts of unbound conjugates at a wavelength of 400 nm (Gemini XS; Molecular Device, Sunnyvale, CA, USA) and subtracting from the total amounts of conjugates.

Characterization of the nanosheets

Atomic force microscopy (AFM) was used to measure the sizes of the surface-modified rGO nanosheets. Pre-cut silicon wafer sections (5 mm×5 mm; Virginia Semiconductor Inc, Fredericksburg, VI, USA) were silanized and immersed in a solution containing rGO nanosheets (10 μg/mL) modified with PC or CPC. The topography, thickness, and lateral sizes were measured using AFM (XE-100; Park Systems, Suwon, Republic of Korea) in non-contact mode. The shapes of the PC/rGO and CPC/rGO particles were examined using transmission electron microscopy (JEM 1010; JEOL Ltd, Tokyo, Japan). To test biological stability, surface-modified nanosheets (0.1 mg) were incubated in 0.8 mL of murine serum for 4 h. The sizes of nanosheets were then measured by dynamic light scattering (ELSZ-1000; Photal, Osaka, Japan). The zeta potentials of rGO, PC/rGO, and CPC/rGO were analyzed after 1 h of incubation in triple-distilled water (TDW) or serum using laser Doppler microelectrophoresis at an angle of 22°.

Singlet oxygen generation of Ce6 upon irradiation

The production of singlet oxygen ($^1O_2$) was measured using a singlet oxygen sensor green reagent (SOSG; Life Technologies, Grand Island, NY, USA) after irradiating each sample. Ce6, PC or CPC (Ce6 10 μg/mL) in free form or surface-modified nanosheets was irradiated using a 660 nm light emitting diode (LED; Mikwang Electronics, Busan, Republic of Korea) with a luminous intensity of 8000 mCd for 20 min. During irradiation, 50 μL aliquots were collected each minute from the 1 mL bulk sample. Each aliquot was then mixed with 2.5 μmol/L of SOSG solution. The presence of singlet oxygen was detected by measuring the fluorescence of the SOSG solution using excitation and emission wavelengths of 504 and 525 nm, respectively, in a fluorescence microplate reader (Gemini XS).

Photothermal properties of the rGO nanosheets

The photothermal properties of the surface-modified nanosheets were measured using an IR thermal imaging system after NIR irradiation of each sample. To mimic *in vivo* conditions, the rGO nanosheets (5 μg/mL) modified with PC or CPC conjugates were pre-warmed at 37 °C before light irradiation. The surface-modified rGO were then irradiated using an 808 nm continuous wave NIR diode laser beam (PSU-FC; ChangChun New Industries Optoelectronics Tech Co, Ltd, Changchun, China) with an output power of 1.5 W. The temperature and photothermal images of the suspensions during laser irradiation were recorded at various time points using an IR thermal imaging system (FLIR T420; FLIR Systems Inc, Danderyd, Sweden).

In vitro release test

The released amounts of CPC from rGO were measured by a dialysis method. In brief, 1 mL of CPC/rGO (4 mg/mL) in a dialysis bag (Spectrum Laboratories, Inc, Rancho Dominguez, CA, USA) was placed in 50 mL of PBS (pH 4.5 or pH 7.4) with 0.2% Tween-80. At various time points, 1 mL of medium was collected and replaced with the same volume of fresh medium. The concentrations of released CPC were measured at an excitation wavelength of 400 nm and an emission wavelength of 660 nm using a fluorescence microplate reader (Gemini XS).

Flow cytometry analysis of the claudin 4 receptors on the tumor cell surfaces

Flow cytometry was used to test for the expression of claudin 4 receptors on the surfaces of U87 glioblastoma or HeLa cervical cancer cell lines (American Type Culture Collection, Rockville, MD, USA). The U87 or HeLa cells were incubated for 1 h at 4 °C together with a fluorescein-conjugated mouse anti-claudin 4 monoclonal antibody (R&D Systems, Inc, Minneapolis, MN, USA) at a dilution of 1:100. Claudin 4-positive cell populations were identified using a BD FACSCalibur system equipped with Cell Quest Pro software (BD Bioscience, San Jose, CA, USA).

Cellular uptake study

The cellular uptake of PC/rGO and CPC/rGO was tested in U87 cells using confocal microscopy and flow cytometry. U87 cells were seeded onto cover glasses at a density of 8×10^4 cells/well in 24 well plates. The next day, the cells were treated with PC/rGO or CPC/rGO nanosheets at a concentration of 50 μmol/L PC or CPC conjugate and 4.8 μg/mL rGO nanosheets. In some experiments, the cellular uptake of CPC/rGO was tested in the presence of CPE30. For competition assays, cells were pre-incubated with 0.5 mmol/L CPE30 for 1 h prior to treatment with CPC/rGO nanosheets. After incubating for 1 h, the cells were washed and fixed with 4%

paraformaldehyde in PBS for 15 min, followed by staining with 4′,6-diamidino-2-phenylindole dihydrochloride (Sigma-Aldrich). The fluorescence intensity of cellular Ce6 was observed using a confocal laser scanning microscope (LSM 5 Exciter; Carl Zeiss, Inc, Jena, Germany). The cells were analyzed using a BD FACSCalibur flow cytometer using the Cell Quest Pro software (BD Bioscience).

Detection of the cellular ROS

The production of cellular ROS was measured using a cell-permeant indicator. U87 cells were seeded onto cover glasses at a density of 8×10^4 cells/well in 24-well plates. The next day, the cells were treated with PC/rGO or CPC/rGO nanosheets at a concentration of 50 μmol/L PC or CPC conjugates and 4.8 μg/mL rGO nanosheets. After incubating for 1 h, the cells were washed and re-suspended in fresh media. The cells were then irradiated using a 660 nm LED (Mikwang Electronics) with a luminous intensity of 8000 mCd for 20 min. After LED irradiation, the cells were re-suspended in pre-warmed PBS containing 10 μmol/L of 2′,7′-dichlorodihyro fluorescein diacetate (Sigma-Aldrich) for 10 min and washed with fresh media. The fluorescence intensity corresponding to the cellular ROS was measured using fluorescence microscopy (Leica DM IL; Leica, Wetzlar, Germany).

In vitro photothermal effects following irradiation

U87 cells were seeded onto cover glasses at a density of 8×10^4 cells/well in 24 well plates. The next day, the cells were treated with PC/rGO or CPC/rGO nanosheets at a concentration of 50 μmol/L of the PC or CPC conjugates and 4.8 μg/mL of the rGO nanosheets. After incubating for 1 h, the cell suspensions were centrifuged at 100×*g* for 3 min and irradiated using an 808 nm continuous wave NIR diode laser at an output power of 1.5 W. The temperature and photothermal images of the cell suspensions during laser irradiation were recorded each minute using an IR thermal imaging system (FLIR T420). The photothermal heating curve of the growth media was obtained as a negative control.

Cell viability assay following dual wavelength irradiation

The viability of cells treated with CPC/rGO and then irradiated at two wavelengths (dual wavelength irradiation) was quantified by a fluorescence-staining live cell assay (Invitrogen Corp, Carlsbad, CA, USA). U87 cells were seeded onto cover glasses at a density of 8×10^4 cells/well in 24 well plates. The next day, the cells were treated with PC/rGO or CPC/rGO nanosheets at a concentration of 50 μmol/L PC or CPC conjugates and 4.8 μg/mL rGO nanosheets. After incubating for 1 h, the cells were irradiated using a 660 nm LED for 20 min and an 808 nm continuous wave NIR diode laser for 3 min. After irradiation, the cells were washed with cold PBS and re-suspended in fresh media for 24 h. Live cell staining was accomplished by adding 2 μmol/L calcein to the cells. After 10 min, the cells were washed twice with PBS and imaged using fluorescence microscopy (Leica DM IL). For quantification of cell viability, fluorescence intensity of calcein was measured at an excitation wavelength of 400 and an emission wavelength of 660 nm using a fluorescence microplate reader (Gemini XS). The cell viability in each group was expressed as a percentage relative to the control cells.

Statistical analysis

ANOVA was used for the statistical evaluation of the experimental data. The Student–Newman–Keuls test was used as a *post hoc* test. All statistical analyses were carried out using SigmaStat software (version 3.5, Systat Software, Richmond, CA, USA), and a P-value <0.05 was considered significant.

Results

Construction and physical properties of the surface-modified rGO nanosheets

The synthesis of PC and CPC conjugates was confirmed by MALDI-TOF (Supplementary Figure S1). Upon irradiation using a 660 nm LED, the production of singlet oxygen by PC (Figure 2B) and CPC (Figure 2C), as indicated by the measured SOSG fluorescence, was higher than free Ce6 (Figure 2A). The morphology and zeta potential were characterized for the CPC/rGO system. The morphology of PC/rGO (Figure 3A, 3C) did not differ from that of CPC/rGO (Figure 3B, 3D).

Incubation of nanosheets in serum did not significantly affect the lateral sizes regardless of surface modification (Figure 3E). The zeta potential values of PC/rGO and CPC/rGO were lower than for rGO in both TDW and serum conditions. After 1 h of serum incubation, the zeta potentials of PC/rGO and CPC/rGO were slightly increased but were still lower than -30 mV (Figure 3F). At a ratio of 2.5:1, the amount of Ce6 conjugates per μg rGO nanosheets was 12.5±1.4 μg for PC and 20.4±3.4 μg for CPC (Supplementary Figure S2). Upon loading to rGO, the production of singlet oxygen by CPC was significantly reduced (Supplementary Figure S3).

Photothermal properties of the surface-modified rGO nanosheets

The PC/rGO and CPC/rGO systems both displayed photothermal properties. The photothermal capacities of PC/rGO and CPC/rGO were similar to that of free rGO. Laser irradiation caused the temperature of the PC/rGO and CPC/rGO solution to increase, as observed in solutions containing free rGO alone (Figure 4).

In vitro release of CPC from rGO

In vitro release of CPC from rGO nanosheets was compared at neutral and acidic conditions mimicking the endosomal environment. Release of CPC from rGO nanosheets was pH-dependent. The release of CPC from rGO nanosheets was faster and occurred to a greater extent at pH 4.5 than at pH 7.4 (Figure 5). In neutral conditions (pH 7.4), the release of CPC gradually increased over 6 h and reached a plateau. However, in acidic conditions (pH 4.5), CPC was gradually released from rGO over 12 h, with higher amounts of CPC released overall compared to the neutral conditions.

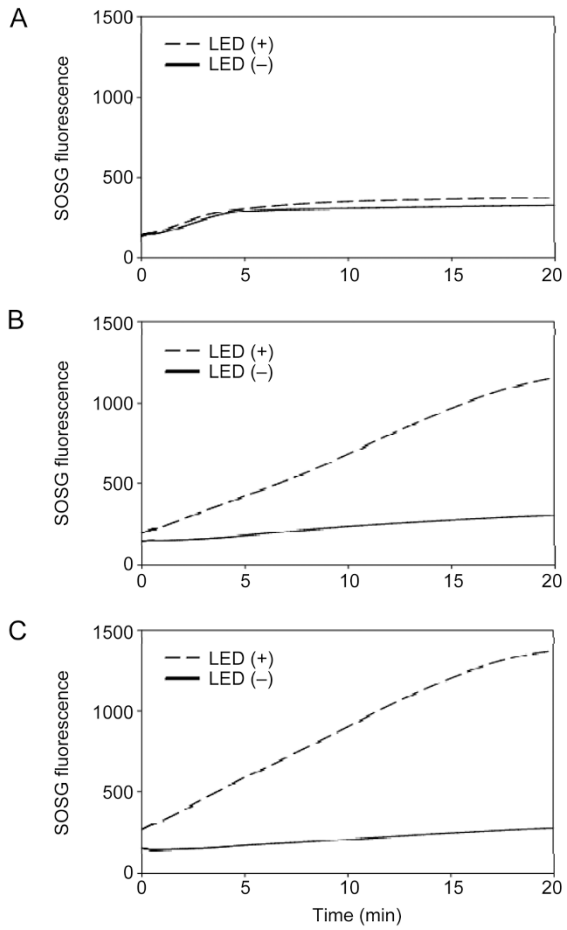

Figure 2. Singlet oxygen production of Ce6 during LED irradiation. The production of singlet oxygen from free Ce6 (A), PC (B), and CPC (C) was observed during LED irradiation.

Cellular uptake of CPC/rGO

The cellular uptake of CPC/rGO was tested in claudin 4-overexpressing U87 glioma cells. FACS analysis using a fluorescent anti-claudin 4 antibody revealed that the U87 cells (Supplementary Figure S4B) but not the HeLa cells (Supplementary Figure S4A) were positive for claudin 4 expression. Uptake of CPC/rGO was significantly higher than that of PC/rGO in U87 cells (Figure 6). To test whether CPC/rGO entered the cells via the same pathway as CPE30, we compared the uptake of CPC/rGO with or without pretreatment with CPE30. Pretreatment with CPE 30 significantly reduced cellular uptake of CPC/rGO. Confocal microscopy (Figure 6A) and flow cytometry data (Figure 6B, 6C) showed that cellular uptake of CPC/rGO was considerably reduced after pretreating claudin 4-overexpressing U87 cells with CPE30.

Dual-photoresponsive properties of CPC/rGO-treated cells

Although PC/rGO and CPC/rGO showed similar photothermal capacities (Figure 4), they differed in cellular uptake efficiency. Irradiation at 660 nm resulted in significant fluorescence quenching (indicating no cellular ROS) in the rGO and PC/rGO groups. By contrast, the fluorescence intensity corresponding to cellular ROS increased significantly in the CPC/

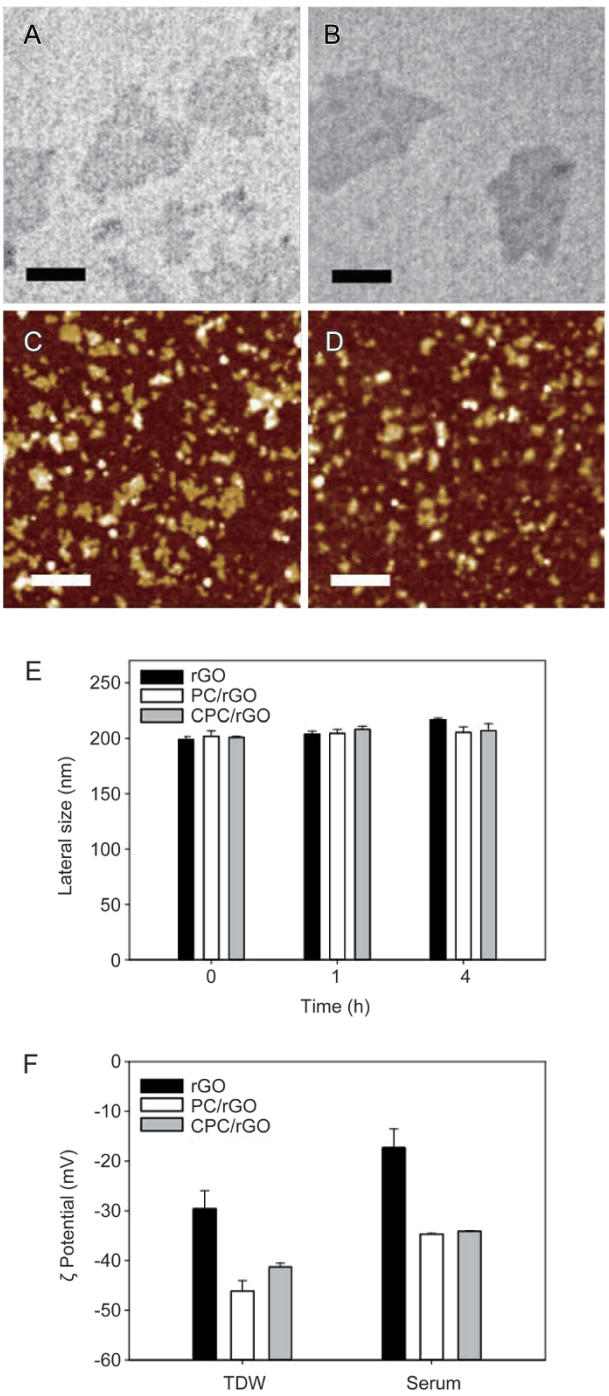

Figure 3. Size and zeta potentials of the surface-modified rGO nanosheets. Transmission electron microscopy images of PC/rGO (A) and CPC/rGO (B) are presented (scale bars indicate 100 nm). AFM images of PC/rGO (C) and CPC/rGO (D) are presented (scale bars indicate 1 μm). (E) The lateral sizes of rGO, PC/rGO, and CPC/rGO were determined after incubation in serum. (F) Zeta potentials of rGO, PC/rGO, and CPC/rGO were determined after incubation in TDW or serum for 1 h.

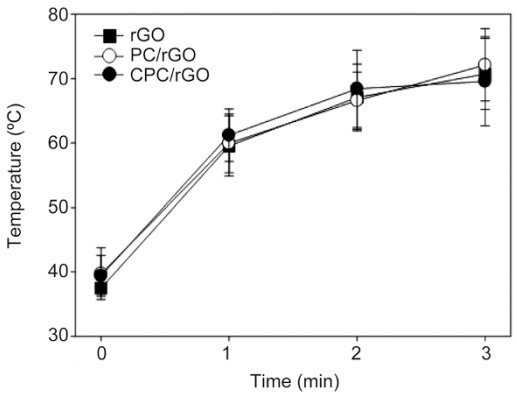

Figure 4. Photothermal activity of the surface-modified rGO nanosheets. The real-time temperature increases of the rGO, PC/rGO, or CPC/rGO were recorded upon irradiation at 808 nm. Results are reported as the mean±SD of three independent experiments.

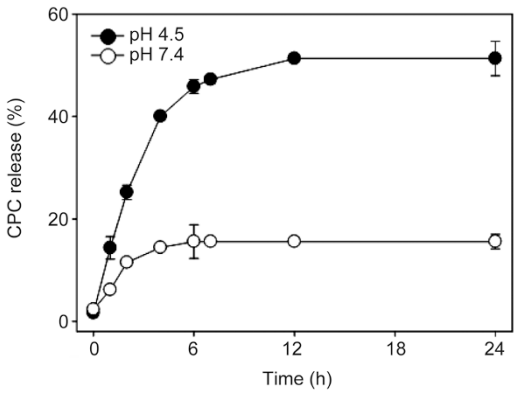

Figure 5. *In vitro* release of CPC from rGO nanosheets. The release of CPC from rGO was measured at acidic and neutral pH conditions. Results are presented as the mean±SD of three independent experiments.

rGO-treated group (Figure 7A). Irradiation at 808 nm resulted in a temperature increase in the CPC/rGO system (Figure 7B). After 3 min of irradiation at 808 nm, the temperature of the CPC/rGO-treated cells was 56.0±2.3 °C (Figure 7C).

Photodynamic and photothermal anticancer effects of CPC/rGO

The photoresponsive anticancer effects of CPC/rGO were dependent on the concentration of CPC (Figure 8A). In the absence of light exposure, there were little differences in the viability among the groups treated with different concentrations of CPC on rGO. In contrast, after irradiation at 660 nm, the viability of cells decreased with increasing concentrations of CPC. Upon dual light exposure, the viability of cells was reduced to 50.5%±1.7% and 7.7%±0.5% after treatment with 25 and 50 μmol/L of CPC on rGO, respectively.

Consistent with the cellular uptake patterns, CPC/rGO, but not rGO or PC/rGO, exhibited enhanced photothermal anticancer activity. In the absence of irradiation, none of the groups displayed significant killing of the U87 cells; however, after 3 min irradiation at 808 nm, the cells treated with CPC/rGO showed higher cell death compared to the groups treated with PC/rGO or rGO alone (Figure 8B). Moreover, a synergistic anticancer effect was observed in CPC/rGO-treated cells upon irradiation at two wavelengths (Figure 8B). Fluorescence staining of live cells revealed that the lowest

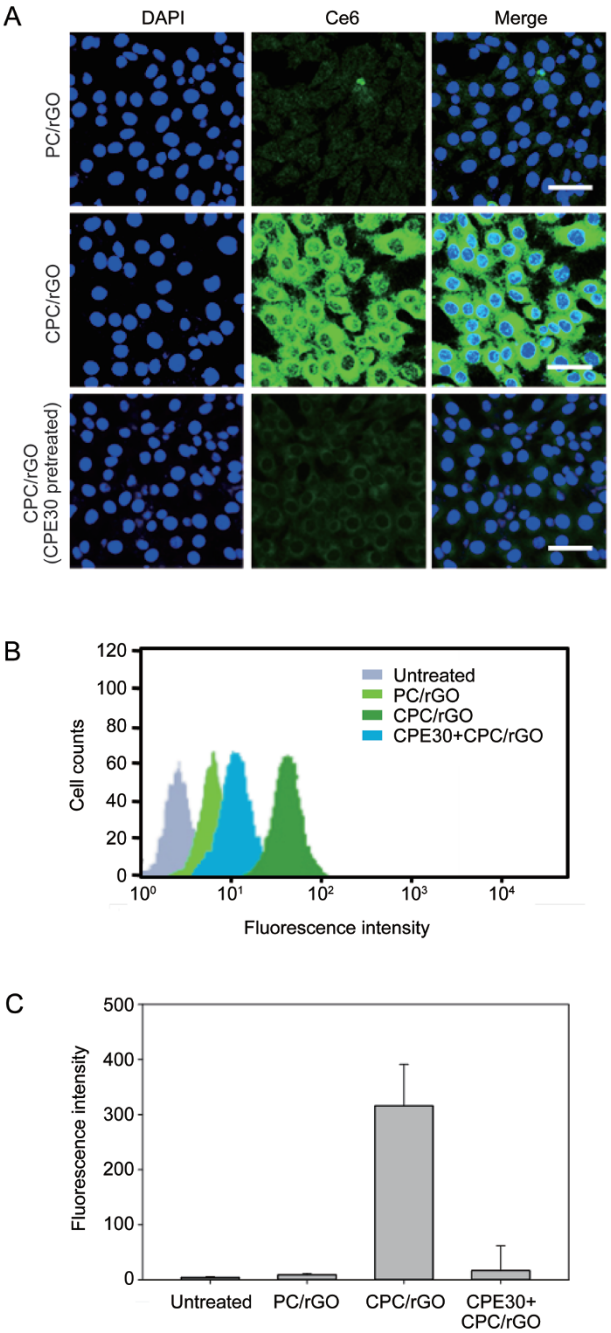

Figure 6. Cellular uptake of CPC/rGO. U87 cells were treated with PC/rGO or CPC/rGO (with or without CPE30 pretreatment). After treatment for 1 h, the fluorescence of Ce6 was measured by confocal microscopy (scale bar indicates 20 μm). Representative flow cytometry data are presented (B), and the fluorescence-positive cell populations were quantified (C). Results are reported as the mean±SD of three independent experiments.

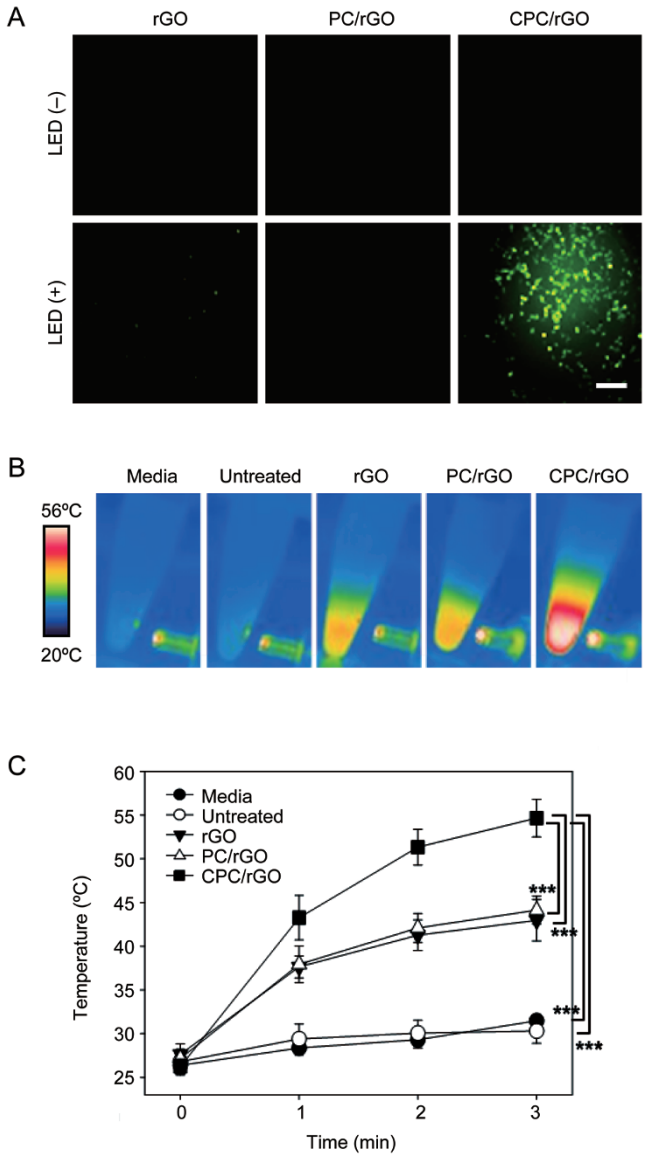

Figure 7. Dual photo-responsiveness of the CPC/rGO-treated cells. U87 cells were treated with rGO, PC/rGO, or CPC/rGO for 1 h. The intracellular ROS accumulation was measured after irradiation at 660 nm (A). The real-time temperature increases were recorded upon irradiation at 808 nm (B). The highest cell suspension temperature was determined using the FLIR QuickReport 1.2 software (C). Results are reported as the mean±SD of three independent experiments. $^{***}P<0.005$ (ANOVA and Student-Newman-Keuls test, $n=5$).

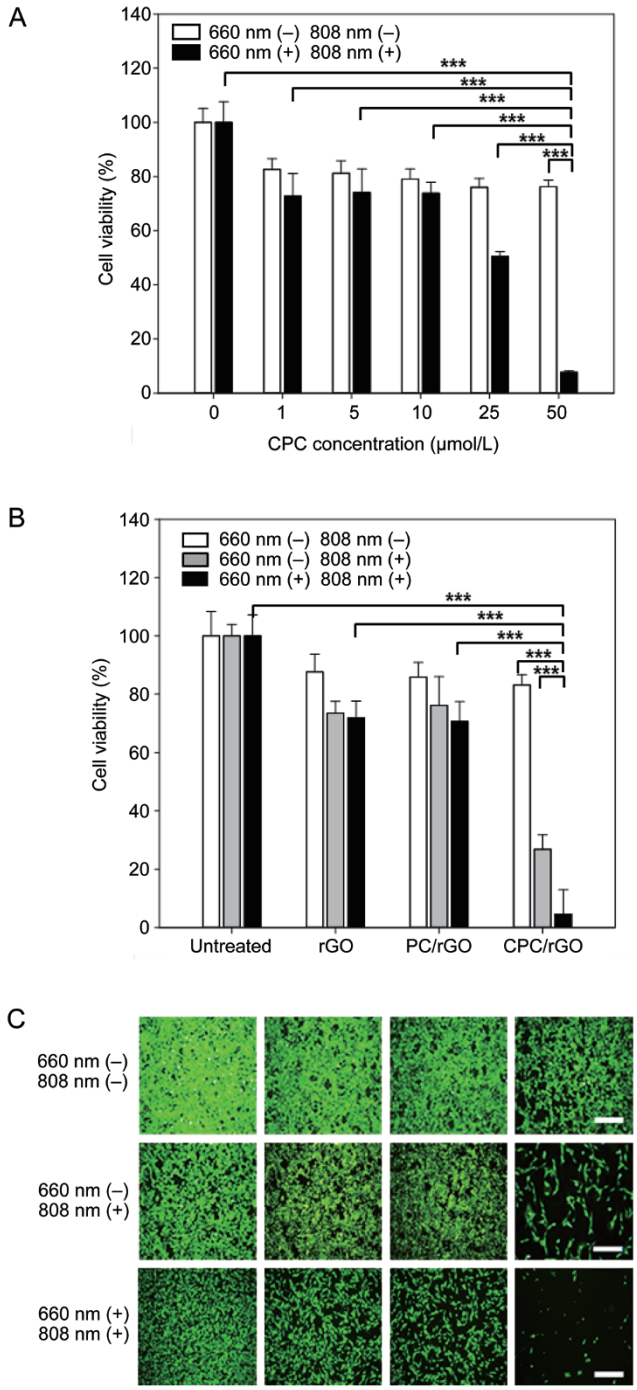

Figure 8. Photodynamic and photothermal anticancer effect. U87 cells were treated with various concentrations of CPC on rGO and irradiated at two wavelengths (660 nm and 808 nm). After 24 h, live cells were stained with calcein and the cell viability was measured using fluorometry (A). U87 cells, either treated or untreated with rGO, PC/rGO, or CPC/rGO, were irradiated at 808 nm or two wavelengths. After 24 h, live cells were stained with calcein and the percentage of viable cells was measured using fluorometry (B) and observed by fluorescence microscopy (C). Results are reported as the mean±SD of three independent experiments. The scale bar indicates 100 μm. $^{***}P<0.005$ (ANOVA and Student-Newman-Keuls test, $n=3$).

population of live cells was present in the group treated with CPC/rGO after irradiation at two wavelengths (Figure 8C).

Discussion

Here, CPE30 was used as a targeting moiety to deliver rGO to claudin 4-overexpressing cells. The CPE30 peptide has been previously reported to bind with a high affinity to the claudin 4 receptor and to internalize to the target cells[7]. Consistent with our observations of claudin 4-overexpressing cells, other

studies have reported overexpressed claudin 4 in glioblastomas[18].

We observed that PC and CPC enhanced the generation of singlet oxygen compared to free Ce6 upon 660 nm irradiation (Figure 2). The exact mechanism for the enhancement remains unclear. One possibility might be the three dimensional configurations of the conjugates, which may increase the photoresponsiveness of the Ce6 moiety. Similar to our observation, a recent study reported an increase of singlet oxygen generation efficiency of Ce6 after conjugation with Pluronic F-127[19]. However, after rGO loading, PC and CPC showed lower generation of singlet oxygen than free Ce6 (Supplementary Figure S3). This phenomenon might result from partial quenching of singlet oxygen by the rGO nanosheets[13, 14, 20].

To anchor CPE30 onto rGO nanosheets, Ce6, as an adsorption and photodynamic agent, was conjugated with PEG and then CPE30 sequentially, resulting in a CPC conjugate. We previously observed that Ce6 adsorbed onto graphene nanosheets and functioned as a PS[17]. Graphene-based nanosheets have been reported to adsorb aromatic drugs, including Ce6, via π–π stacking and hydrophobic interactions[21]. PEG was used as a spacer between CPE30 and Ce6. PEG stabilized the rGO dispersion and reduced the adsorption of CPE30 onto rGO. Moreover, the presence of PEG in PC or CPC may contribute to the stability of the surface-modified nanosheets in serum. Indeed, we observed that the sizes of PC/rGO and CPC/rGO were retained in serum (Figure 3E).

In this study, we used a ratio of 2.5:1 for PC/rGO and CPC/rGO. The ratio was chosen to provide the highest loading efficiency and amount of Ce6 per rGO nanosheet. At ratios of 5:1 or 10:1, we observed increased fluorescence intensity of the conjugate and rGO mixtures due to excess amounts of unbound conjugate. Excess free conjugate at ratios higher than 5:1 might be due to the saturation of Ce6 binding to rGO at the ratio of 2.5:1.

The higher cellular uptake of CPC/rGO by U87 cells supported the notion that the CPE30 moiety in CPC/rGO played a role in the claudin 4 receptor-mediated cellular delivery of rGO nanosheets (Figure 6). As a claudin 4 receptor binds ligand peptides, the cell undergoes endocytosis, a crucial mechanism for nanocarriers to achieve cellular entry. Fluorescence microscopy and flow cytometry of the cells treated with CPC/rGO (Figure 6) indicated the recovery of Ce6 fluorescence after endocytosis. Previously, we[17] and others[22] observed dequenching of Ce6 fluorescence after cellular delivery using graphene-based nanosheets. Such recovery of Ce6 fluorescence after endocytosis might be attributed to the liberation of Ce6 from graphene-based nanosheets by protonation and weakened π–π interactions with rGO at acidic endosomes[22]. Indeed, we observed that the release rate of CPC from rGO nanosheets was higher in acidic conditions than in a neutral environment (Figure 5).

In this study, we observed that CPE30-mediated targeting enabled the CPC/rGO system to deliver a specific photoresponsive agent to claudin 4-overexpressing cells. Although CPE30 is reported to bind to claudin 4 receptors on several types of tumor cells[7], few studies have employed the targeting properties of CPE30 in tumor cell-directed delivery systems. The notable reduction of cellular uptake of CPC/rGO after pretreatment with CPE30 supports the idea that CPC/rGO were taken up by claudin 4 receptor-mediated endocytosis (Figure 6). The competition assay results indicate that the presence of CPE30 in CPC conjugates may have contributed to overcoming the cellular uptake-limiting PEG dilemma[23], and provide claudin 4 receptor-specific delivery.

Dual photoresponsiveness was achieved by anchoring photodynamic Ce6 to photothermal rGO. The dual photoresponsiveness approach was investigated by loading a PS onto the graphene-based nanosheets. Graphene oxide nanosheets have been electrostatically loaded with methylene blue, a hydrophilic and positively charged PS, for use in combined phototherapy[14]. Our CPC/rGO system provided evidence that a physically adsorbed PS may serve as an anchoring moiety for multifunctional ligands.

For the dual phototherapy, the combination of irradiation time needs to be optimized to provide the highest therapeutic effect. In this study, the irradiation times for photodynamic and photothermal effect were 20 and 3 min, respectively. The light exposure times were chosen based on the photoresponsive effect of each. Singlet oxygen production efficiency was observed to reach the highest value after 20 min of exposure at 660 nm (Figure 2). The photothermal effect of rGO nanosheets reached the maximum temperature after 3 min of exposure at 808 nm (Figure 4). Based on these observations, we combined a light exposure time for two wavelengths to provide the maximal photodynamic and photothermal effect (Figure 8).

In this study, we report the development of claudin 4-specific photodynamic and photothermal systems using a PS Ce6 to anchor the claudin 4 ligand peptides onto rGO nanosheets. Modifying the surfaces of the rGO nanosheets with CPE30 enhanced cellular uptake by claudin 4 receptor-overexpressing cells. Ce6, as a CPE30 anchoring moiety, can be used to generate cellular ROS and achieve a photodynamic anticancer effect. The enhanced cellular uptake of rGO nanosheets upon attachment to the CPE30 moiety provided enhanced photothermal anticancer effects. Although this study demonstrated the feasibility of designing target-specific dual photodynamic and photothermal agents for use in U87 cells, the design may be applied to other cancer cells using other targeting moieties in place of CPE30. Tumor-targeted dual photomedicines could potentially be developed to have enhance anticancer effects by combining photodynamic and photothermal effects with irradiation at different wavelengths.

Acknowledgements

This work was supported by research grants from the Ministry of Science, ICT and Future Planning, Republic of Korea (NRF-2015R1A2A1A01005674) and from the Korean Health Technology R&D Project (No HI15C2842), Ministry of Health & Welfare, Republic of Korea.

Supplementary information

Supplementary information is available on the website of Acta Pharmacologica Sinica.

References

1 Zhang Z, Wang J, Chen C. Near-infrared light-mediated nanoplatforms for cancer thermo-chemotherapy and optical imaging. Adv Mater 2013; 25: 869–80.
2 Idris NM, Gnanasammandhan MK, Zhang J, Ho PC, Mahendran R, Zhang Y. *In vivo* photodynamic therapy using upconversion nanoparticles as remote-controlled nanotransducers. Nat Med 2012; 18: 1580–5.
3 Agostinis P, Berg K, Cengel KA, Foster TH, Girotti AW, Gollnick SO, *et al*. Photodynamic therapy of cancer: an update. CA Cancer J Clin 2011; 61: 250–81.
4 Miao W, Shim G, Kim G, Lee S, Lee HJ, Kim YB, *et al*. Image-guided synergistic photothermal therapy using photoresponsive imaging agent-loaded graphene-based nanosheets. J Control Release 2015; 10: 28–36.
5 Kwon MH. Emerging roles of claudins in human cancer. Int J Mol Sci 2013; 14: 18148–80.
6 Saitoh Y, Suzuki H, Tani K, Nishikawa K, Irie K, Ogura Y, *et al*. Structural insight into tight junction disassembly by *Clostridium perfringens* enterotoxin. Science 2015; 347: 775–8.
7 Cocco E, Casagrande F, Bellone S, Richter CE, Bellone M, Todeschini P, *et al*. *Clostridium perfringens* enterotoxin carboxy-terminal fragment is a novel tumor-homing peptide for human ovarian cancer. BMC Cancer 2010; 10: 349.
8 Robinson JT, Tabakman SM, Liang Y, Wang H, Casalongue HS, *et al*. Ultrasmall reduced graphene oxide with high near-infrared absorbance for photothermal therapy. J Am Chem Soc 2011; 133: 6825–31.
9 Miao W, Shim G, Lee S, Oh YK. Structure-dependent photothermal anticancer effects of carbon-based photoresponsive nanomaterials. Biomaterials 2014; 35: 4058–65.
10 Kim HS, Lee DY. Photothermal therapy with gold nanoparticles as an anticancer medication. J Pharm Invest 2017; 47: 19–26.
11 Yang K, Xu H, Cheng L, Sun C, Wang J, Liu Z. *In vitro* and *in vivo* near-infrared photothermal therapy of cancer using polypyrrole organic nanoparticles. Adv Mater 2012; 24: 5586–92.
12 Shim G, Kim JY, Han J, Chung SW, Lee S, Byun Y, *et al*. Reduced graphene oxide nanosheets coated with an anti-angiogenic anticancer low-molecular-weight heparin derivative for delivery of anticancer drugs. J Control Release 2014; 189: 80–9.
13 Tian B, Wang C, Zhang S, Feng L, Liu Z. Photothermally enhanced photodynamic therapy delivered by nano-graphene oxide. ACS Nano 2011; 5: 7000–9.
14 Sahu A, Choi WI, Lee JH, Tae G. Graphene oxide mediated delivery of methylene blue for combined photodynamic and photothermal therapy. Biomaterials 2013; 34: 6239–48.
15 Hong EJ, Choi DG, Shim MS. Targeted and effective photodynamic therapy for cancer using functionalized nanomaterials. Acta Pharm Sin B 2016; 6: 297–307.
16 Hu FQ, Jiang XH, Huang X, Wu XL, Yuan H, Wei XH, *et al*. Enhanced cellular uptake of chlorine e6 mediated by stearic acid-grafted chitosan oligosaccharide micelles. J Drug Target 2009; 17: 384–91.
17 Miao W, Shim G, Lee S, Lee S, Choe YS, Oh YK. Safety and tumor tissue accumulation of pegylated graphene oxide nanosheets for co-delivery of anticancer drug and photosensitizer. Biomaterials 2013; 34: 3402–10.
18 Rangel LB, Agarwal R, D'Souza T, Pizer ES, Alò PI, Lancaster WD, *et al*. Tight junction proteins claudin-3 and claudin-4 are frequently over-expressed in ovarian cancer but not in ovarian cystadenomas. Clin Cancer Res 2003; 9: 2567–75.
19 Park H, Na K. Conjugation of the photosensitizer Chlorin e6 to pluronic F127 for enhanced cellular internalization for photodynamic therapy. Biomaterials 2013; 34: 6992–7000.
20 Cao J, An H, Huang X, Fu G, Zhuang R, Zhu L, *et al*. Monitoring of the tumor response to nano-graphene oxide-mediated photothermal/photodynamic therapy by diffusion-weighted and BOLD MRI. Nanoscale 2016; 8: 10152–9.
21 Rong P, Yang K, Srivastan A, Kiesewetter DO, Yue X, Wang F, *et al*. Photosensitizer loaded nano-graphene for multimodality imaging guided tumor photodynamic therapy. Theranostics 2014; 4: 229–39.
22 Huang P, Xu C, Lin J, Wang C, Wang X, Zhang C, *et al*. Folic acid-conjugated graphene oxide loaded with photosensitizers for targeting photodynamic therapy. Theranostics 2011; 1: 240–50.
23 Kim CH, Lee SG, Kang MJ, Lee S, Choi YW. Surface modification of lipid-based nanocarriers for cancer cell-specific drug targeting. J Pharm Invest 2017; 47: 203–27.